New Journal of Physics
The open access journal at the forefront of physics

Deutsche Physikalische Gesellschaft DPG IOP Institute of Physics

PAPER • OPEN ACCESS

Multi-spinon and antiholon excitations probed by resonant inelastic x-ray scattering on doped one-dimensional antiferromagnets

To cite this article: Umesh Kumar *et al* 2018 *New J. Phys.* **20** 073019

New Journal of Physics
The open access journal at the forefront of physics

Deutsche Physikalische Gesellschaft DPG
IOP Institute of Physics

Published in partnership with: Deutsche Physikalische Gesellschaft and the Institute of Physics

OPEN ACCESS

RECEIVED
7 May 2018

REVISED
27 June 2018

ACCEPTED FOR PUBLICATION
29 June 2018

PUBLISHED
11 July 2018

PAPER

Multi-spinon and antiholon excitations probed by resonant inelastic x-ray scattering on doped one-dimensional antiferromagnets

Umesh Kumar[1,2,4], **Alberto Nocera**[1,3], **Elbio Dagotto**[1,3] and **Steve Johnston**[1,2]

[1] Department of Physics and Astronomy, The University of Tennessee, Knoxville, TN 37996, United States of America
[2] Joint Institute for Advanced Materials, The University of Tennessee, Knoxville, TN 37996, United States of America
[3] Materials Science and Technology Division, Oak Ridge National Laboratory, Oak Ridge, TN 37831, United States of America
[4] Author to whom any correspondence should be addressed.

E-mail: ukumar2@vols.utk.edu

Keywords: holon, spinon, antiferromagnetism, 1D strongly correlated systems

Supplementary material for this article is available online

Abstract

Resonant inelastic x-ray scattering (RIXS) at the oxygen *K*-edge has recently accessed multi-spinon excitations in the one-dimensional antiferromagnet (1D-AFM) Sr_2CuO_3, where four-spinon excitations are resolved separately from the two-spinon continuum. This technique, therefore, provides new opportunities to study fractionalized quasiparticle excitations in doped 1D-AFMs. To this end, we carried out exact diagonalization studies of the doped *t*–*J* model and provided predictions for oxygen *K*-edge RIXS experiments on doped 1D-AFMs. We show that the RIXS spectra are rich, containing distinct two- and four-spinon excitations, dispersive antiholon excitations, and combinations thereof. Our results highlight how RIXS complements inelastic neutron scattering experiments by accessing additional charge and spin components of fractionalized quasiparticles.

1. Introduction

One-dimensional (1D) magnetic systems have attracted considerable interest throughout the scientific community for more than half a century. This interest stems from the fact that these systems provide excellent opportunities to study novel quantum phenomena such as quasiparticle fractionalization or quantum criticality. Moreover, model Hamiltonians of 1D systems can often be solved exactly using analytical or numerical techniques, making them ideal starting points for understanding the physics of strongly correlated materials. For example, the exact solution of the 1D Hubbard model by Lieb and Wu [1] represented a breakthrough in the field, showing that interacting electrons confined to 1D are characterized by spin-charge separation, where electronic quasiparticle excitations *break* into collective density fluctuations carrying either spinless charge ('(anti)/holons') or chargeless spin ('spinons') quantum numbers with different characteristic energy scales. This work inspired an intense search for materials showing spin-charge separation, but it has only been in the last two decades that this phenomenon was observed [2–7].

Resonant inelastic x-ray scattering (RIXS) [8] has evolved as an important tool for studying the magnetic excitations in correlated materials [9–11], complementing inelastic neutron scattering (INS). RIXS, however, is also a powerful probe of orbital and charge excitations, as was succinctly demonstrated by the experimental observation of spin-orbital fractionalization in a Cu *L*-edge RIXS study of Sr_2CuO_3[12, 13]. Sr_2CuO_3 contains 1D chains of corner-shared CuO_4 plaquettes (see figure 1(c)), where a single hole occupies each Cu $3d_{x^2-y^2}$ orbital, forming a quasi-1D spin-$\frac{1}{2}$ chain. Due to a very weak interchain interaction, the CuO_3 chains decouple above the bulk ordering temperature $T_N = 5.5$ K and form a nearly ideal realization of a 1D antiferromagnet (AFM) [14]. A recent O *K*-edge RIXS study [15] of undoped Sr_2CuO_3 directly observed multi-spinon excitations outside of the two-spinon (2S) continuum (see also figure 1) further highlighting the potential for RIXS to probe such excitations.

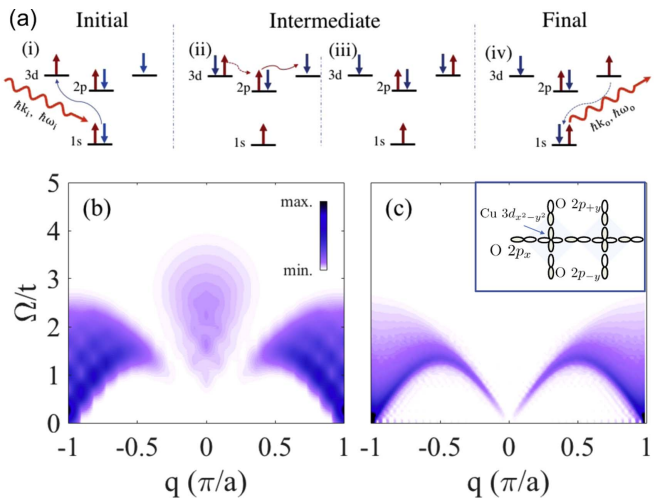

Figure 1. (a) A sketch of the spin-flip mechanism in oxygen *K*-edge RIXS. Hybridization between the Cu and O orbitals allows an incident photon to excite an O 1*s* electron into the $3d_{x^2-y^2}$ orbital on one of the two neighboring Cu sites, creating a Cu d^{10} upper Hubbard band excitation in the intermediate state (subpanel (i)). The d^{10} excitation can transfer to the other neighboring Cu site via two Cu–O hopping processes ((subpanel (ii)) and (subpanel (iii))). Finally, the extra electron decays back into the O 1*s* core level, leaving the system in a final state with a double spin-flip (subpanel (iv)). Inset in panel (c) shows the CuO_4 plaquettes of Sr_2CuO_3 in which only the bridging oxygen participates in the spin-flip process. (b) Computed RIXS spectra for an undoped t–J model on a 22-site chain. (c) $S(q, \omega)$ for an undoped 80-site chain, calculated with DMRG for the same model. Note the additional spectral weight in the RIXS intensity centered at $q = 0$, and absent in $S(q, \omega)$.

To date, spin-charge separation has not been observed using RIXS [13]. In this paper, we performed exact diagonalization (ED) and density matrix renormalization group (DMRG) [16, 17] calculations to show that RIXS measurements on doped 1D AFMs can fill this need. Specifically, we show that O *K*-edge RIXS can access multi-spinon excitations, antiholon excitations, and combinations thereof, thus providing a unique view of spin-charge separation in doped 1D AFMs. Since Sr_2CuO_3 can be doped with Zn, Ni, or Co [18, 19], this material can be used to test our predictions. Moreover, we expect our results to be valid for other 1D doped AFMs, such as Ca_2CuO_3 and $SrCuO_2$, and are not just restricted to Sr_2CuO_3.

Magnetic Scattering at the O K-edge—Before proceeding, we review how magnetic excitations occur in the O *K*-edge ($1s \rightarrow 2p$) [20] measurements on Sr_2CuO_3, as sketched in figure 1(a). Sr_2CuO_3 is a charge-transfer insulator and the ground state character of the CuO_4 plaquettes is predominantly of the form $\alpha|d^9\rangle + \beta|d^{10}\underline{\mathrm{L}}\rangle$ ($\alpha^2 \approx 0.64$, $\beta^2 \approx 0.36$) [21, 22], due to hybridization between the Cu $3d_{x^2-y^2}$ and O 2*p* orbitals. Here, $\underline{\mathrm{L}}$ denotes a hole on the ligand O orbitals. Due to this hybridization, the incident photon can excite an O 1*s* core electron into the Cu 3*d* orbital when tuned to the O *K*-edge, creating an upper Hubbard band excitation. In the intermediate state, the d^{10} configuration can move to the neighboring Cu ion via the bridging O orbital. Since the adjacent Cu orbital also hybridizes with the O containing the core-hole, one of the d^{10} electrons can then decay to fill it, creating a final state with a double spin-flip.

The dynamics in the intermediate state are essential for generating magnetic excitations at this edge, and this is a fundamental difference in how RIXS and INS probe magnetic excitations. One of the advantages of working at the O *K*-edge is that it has relatively long core-hole lifetimes ($\hbar/\Gamma_n$, $\Gamma_n = 0.15$ eV [23]) in comparison to other edges ($\Gamma_n = 1.5$ eV at the Cu *K*-edge and 0.3 eV at the Cu L_3-edge [24]), which provides a longer window for generating magnetic excitations [15, 25]. Because of this, inclusion of the intermediate states in the modeling is necessary. Several efforts addressing the spin dynamics in RIXS have mostly used the *ultrashort core-hole lifetime* (UCL) approximations, which applies to edges with short core-hole lifetimes [26, 27], while studies of 1D systems beyond UCL approximations have been limited [24, 28]. Reference [28] studied the effect of incidence energy on spin dynamics RIXS spectra in 1D using small cluster ED, but a systematic analysis of the incident energy dependence was not carried out. As a result, the multi-spinon excitations at $q = 0$ were not reported. Similarly, [29] discussed the doping dependence of the RIXS spectrum for the t–J model by evaluating the spin response, but the charge response along with the intermediate state dynamics were left out. For these reasons, the prior studies could not address the physics reported here.

2. Model and methods

Sr_2CuO_3 is a multiorbital system, and a multiorbital Hamiltonian should be employed if one wishes to capture the RIXS spectra at all energies. However, our focus here is on the low-energy magnetic and charge excitations

that arise from quasiparticle fractionalization. Prior work at the Cu L-edge showed that the dd- and charge-transfer excitations in Sr_2CuO_3 appear at higher energy losses ($\Omega > 1.5$ eV) [12]. Based on this observation, we work with an effective 1D t–J model, where these interorbital excitations have been integrated out, with the caveat that we will restrict ourselves to energy losses below 1.2 eV (i.e. $4t$). The fact that this same model accurately captures the low-energy the magnetic excitations observed in undoped Sr_2CuO_3 [15], provides further support for this approach. The model Hamiltonian is

$$H = -t\sum_{i,\sigma}(\tilde{d}^{\dagger}_{i,\sigma}\tilde{d}_{i+1,\sigma} + \text{h.c.}) + J\sum_{i}(\mathbf{S}_i \cdot \mathbf{S}_{i+1} - \frac{1}{4}n_i n_{i+1}).$$

Here, $\tilde{d}_{i,\sigma}$ is the annihilation operator for a hole with spin σ at site i, under the constraint of no double occupancy, $n_i = \sum_\sigma n_{i,\sigma}$ is the number operator, and $\mathbf{S}_i$ is the spin operator at site i.

During the RIXS process [8], an incident photon with momentum $\mathbf{k}_{\text{in}}$ and energy ω_{in} ($\hbar = 1$) tuned to an elemental absorption edge resonantly excites a core electron into an unoccupied state in the sample. The resulting core-hole and excited electron interact with the system creating several elementary excitations before an electron radiatively decays into the core level, emitting a photon with energy ω_{out} and momentum $\mathbf{k}_{\text{out}}$. The RIXS intensity is given by the Kramers–Heisenberg formula [8]

$$I = \sum_f \left| \sum_n \frac{\langle f|D^{\dagger}|n\rangle\langle n|D|i\rangle}{E_i + \omega_{\text{in}} - E_n + i\Gamma_n} \right|^2 \delta(E_f - E_i - \Omega), \tag{1}$$

where $\Omega = \omega_{\text{in}} - \omega_{\text{out}}$ is the energy loss, $|i\rangle$, $|n\rangle$, and $|f\rangle$ are the initial, intermediate, and final states of the RIXS process with energies E_i, E_n, and E_f, respectively, and D is the dipole operator for the O $1s \rightarrow 2p$ transition. In the downfolded t–J model D takes the effective form

$$D = \sum_{i,\sigma} e^{i\mathbf{k}_{\text{in}}\cdot(\mathbf{R}_i + \mathbf{a}/2)}[(\tilde{d}_{i,\sigma} - \tilde{d}_{i+1,\sigma})s^{\dagger}_{i+\frac{1}{2},\sigma} + \text{h.c.}],$$

where $\mathbf{q}$ ($= \mathbf{k}_{\text{out}} - \mathbf{k}_{\text{in}}$) is the momentum transfer and the relative sign is due to the phases of the Cu $3d_{x^2-y^2}$ and O $2p_x$ orbital overlaps along the chain direction. Here, $s_{i+\frac{1}{2},\sigma}$ is the hole annihilation operator for the $1s$ core level on the O atom bridging the i and $i+1$ Cu sites.

By definition, the x-ray absorption scattering (XAS) spectra is given by

$$I_{\text{XAS}} = \sum_n |\langle n|D|i\rangle|^2 \delta(E_n - E_g - \omega_{\text{in}}). \tag{2}$$

At the oxygen K-edge, the evaluation of XAS spectra, prior to RIXS calculation is important to get the appropriate ω_{in}. The dependence of the RIXS spectra on incident energy is discussed in section 3.2.1.

In the real material, the core-hole potential raises the on-site energy of the bridging oxygen orbital (in hole language) in the intermediate state while exerting a minimal influence on the Cu sites. This change locally modifies the superexchange interaction between the neighboring Cu atoms [30]. To account for this effect, we reduce the value of $J_{i,i+1} = J/2$ when solving for the intermediate states, where the core-hole is created on the O atom bridging the i and $i+1$ sites. Our results are not sensitive to reasonable changes in this value as shown in appendix A.

Throughout we set $t = 1$ as our unit of energy ($t \approx 300$ meV in Sr_2CuO_3). The remaining parameters are $\Gamma_n = \frac{1}{2}t$ for all n and $J = \frac{5}{6}t$, unless otherwise stated. These values are typical for the O K-edge measurements of Sr_2CuO_3. The *superexchange* J for Sr_2CuO_3 was reported to be around 250 meV by prior INS and RIXS studies [12, 15, 22]. For Sr_2CuO_3 and closely related 1D cuprate $SrCuO_2$, the hopping t was reported to be 300–600 meV [2, 4, 5, 15, 31]. Also, as further discussed in section 3.2.2, our calculated spectra do not change qualitatively in the range of reported values of t. The inverse core-hole lifetime Γ_n for oxygen K-edge is 150 meV [23]. We also introduce a Gaussian broadening ($\Gamma = \frac{1}{3}t$) for energy conserving δ-function appearing in equation (1). We evaluated equation (1) on a $L = 20$ site chain using the Lanczos method with a fixed filling.

To help identify the relevant charge and spin excitations in the RIXS spectra, we also performed DMRG simulations [16, 17] for the dynamical charge $N(q,\omega)$ and spin $S(q,\omega)$ structure factors on an $L = 80$ site chain, and using correction-vector method [32, 33]. Within the correction-vector approach, we used the Krylov decomposition [34] instead of the conjugate gradient. In the ground state and dynamic DMRG simulations, we used a maximum of $m = 1000$ states, keeping the truncation error below 10^{-8} and used a broadening of the correction-vector calculation $\eta = 0.08t$. The computer package dmrg++ developed by G Alvarez, CNMS, ORNL, was used in the DMRG simulations [35].[5]

[5] See supplementary materials available online at stacks.iop.org/NJP/20/073019/mmedia.

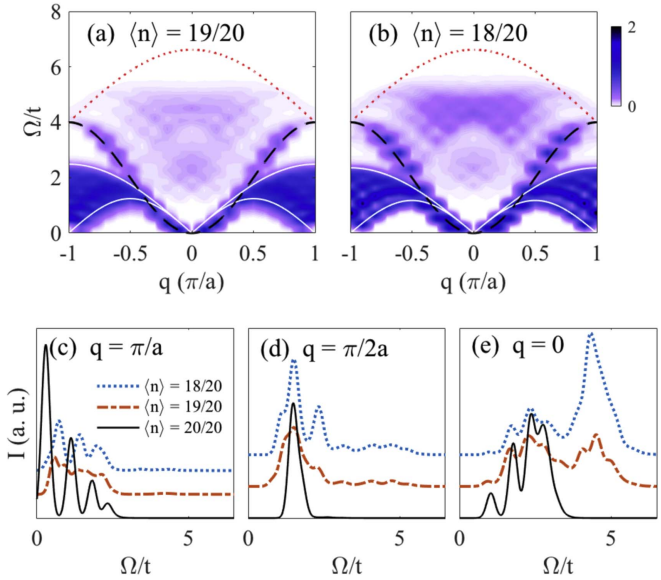

Figure 2. Calculated RIXS spectra at $\omega_{in} = 3t$ for a $L = 20$ site doped t–J chain with (a) one and (b) two additional doped electrons. The white, black, and red lines shows the boundaries for two-spinon continuum, the dispersion of the antiholonic excitation, and upper boundary for antiholon-2S excitations, respectively. Panels (c)–(e) compare the doped RIXS spectra with the undoped case for momentum transfers of $q = \pi/a, q = \pi/(2a)$, and $q = 0$, respectively.

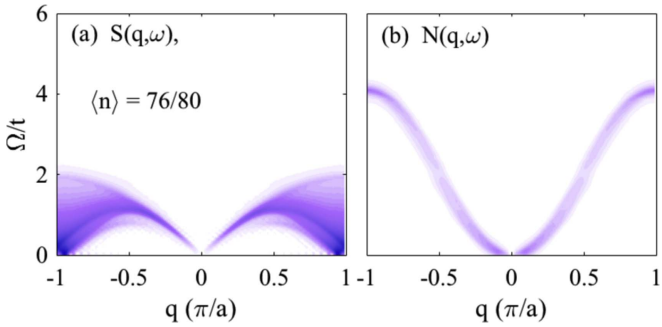

Figure 3. DMRG results for (a) $S(q, \omega)$ and (b) $N(q, \omega)$ for the doped t–J model on a $L = 80$ sites chain and $\langle n \rangle$=0.95 doping.

3. Results

3.1. Undoped RIXS spectra

Figure 1(b) shows the RIXS intensity for the half-filled t–J chain, reproduced from [15]. For comparison, figure 1(c) shows $S(q, \omega)$ obtained using DMRG for the same parameters. The RIXS intensity has two main features. The first is a continuum of excitations that closely mirrors $S(q, \omega)$ and is situated within the boundaries of the 2S continuum. Its intensity is relatively independent of the incident photon energy and is associated primarily with 2S excitations [15, 36]. The second feature is a continuum of excitations laying outside of the 2S continuum, corresponding to 4S excitations. Its intensity is sensitive to both the incident photon energy and the core-hole lifetime, indicating that the intermediate state plays a critical role in creating those excitations [15].

3.2. Doped RIXS spectra

We now turn our attention to the results for the doped case. Figures 2(a) and (b) show the RIXS intensity obtained on a 20-site chain at 5% and 10% electron doping, respectively. Here, we have used $\omega_{in} = 3t$ to enhance the intensity of the features appearing at $q = 0$. To help us better understand the main features, we also computed $S(q, \omega)$ (figure 3(a)) and $N(q, \omega)$ (figure 3(b)) for 5% doping using DMRG.

The RIXS spectra for the doped cases have three recognizable sets of features: (i) a continuum that mirrors the $S(q, \omega)$ in figure 3(a); (ii) a cosine-like dispersive feature with a bandwidth of $4t$ that mirrors $N(q, \omega)$ in figure 3(b); and (iii) two continua, centered at $q = 0$ and extending up to $\sim 6t$ in energy loss. These features are absent in $S(q, \omega)$ and $N(q, \omega)$. The excitations (i) and (ii) point to a manifestation of spin-charge separation in

that the response *bifurcates* into primarily two-spinon (i) and antiholon (ii) excitations, characterized by different energy scales. Also, notice that the dispersions of various peaks in figures 2(a) and (b) do not vary significantly with a small change in doping, except for their relative intensities. It is important to note that the RIXS and $N(q, \omega)$ are response functions that probe excitations with net charge zero, and one would expect to see a holon–antiholon continuum [37]. However, for small electron doping, the holon–antiholon continuum appears effectively as a single antiholon excitation band due to phase space constraints in the holon scattering. For larger electron dopings, we expect to see a distinct holon–antiholon continuum in both RIXS and $N(q, \omega)$.

Figures 2(c)–(e) compare the doping evolution of the RIXS features at fixed momentum points. Figure 2(c) shows line-cut at $q = \pi/a$, where the upper bound (πJ) of the spin excitations decreases upon doping. Similarly, the line-cut at $q = \pi/2a$ in 2(d) shows that the lower bound ($\pi J/2$) of the 2S continuum also decreases with doping, allowing for final states below the 2S continuum of the undoped case. We also observe a secondary feature at higher energy loss due to changes in the holon branch and 4S excitations. Figure 2(e) shows a cut at $q = 0$, where two distinct sets of peaks are clear. The group at lower energy losses appears in the same energy range of the multi-spinon peak observed in the undoped case. The peaks at higher energy loss appear above $\Omega = 4t$ and are identified below. Also, panels (c)–(e) illustrate that the RIXS intensity of spin excitations 2S and 4S gets suppressed upon doping, showing much broader spectral features. Instead, the antiholonic features, that are absent in the undoped case, are enhanced as doping is increased.

The calculated spectra can be understood by making use of the spin-charge separation picture: in 1D, the wavefunction of the large U Hubbard model for N electrons in L lattice sites is a product of 'spinless' charge and 'chargeless' spin wavefunctions [38–40]. The dispersion of charge excitations is given by $\omega_{\bar{h}}(k_{\bar{h}}) = 2t\,(1 - \cos(k_{\bar{h}}a))$ [41, 42], which agrees well with the dispersion observed for feature (ii) (see black dashed line) and in $N(q, \omega)$. As shown in the appendix B, the $N(q, \omega)$ computed here for small *electron doping* is identical to the $N(q, \omega)$ obtained for a 1D spinless fermions chain with the same *fermionic filling*, supporting the spin-charge separation picture. This result indicates that the charge excitation is behaving like a nearly free spinless quasiparticle, i.e. a holon/antiholon. Concerning the spin part, the dispersion relation for a single spinon is given by $\omega_s(k_s) = \frac{\pi}{2}J|\sin(k_s a)|$. Due to the RIXS selection rules, these spin excitations must be generated in even numbers, resulting in a continuum whose boundaries are defined by this dispersion relation. At small doping, the limits of this continuum are modified, which is accounted for using a slightly modified superexchange $\tilde{J} = J\langle n\rangle$ [40]. The upper and lower boundaries of the modified 2S continuum are indicated by the white lines in figure 2 and agree well with the observed excitations.

We can summarize the picture emerging from our results as follows: the 2S-like continuum present in the RIXS spectrum is a pure magnetic excitation as it compares well with the $S(q, \omega)$ from DMRG. The dispersing cosine-like feature in the doped RIXS spectra compares well with the $N(q, \omega)$ from DMRG. We have verified that the $N(q, \omega)$ of the spinless fermions with occupations equal to the electron doping considered above are qualitatively similar to the results obtained for the doped t–J chain as discussed in appendix B. We therefore assign this feature to purely charge-like antiholon excitations.

The peaks at $q = 0$ of the RIXS spectrum are not captured by either $S(q, \omega)$ or $N(q, \omega)$. The lower continuum resembles the multi-spinon continuum [15] also observed in the undoped case, and we, therefore, associate it with 4S excitations. Conversely, the continuum of excitations at energy losses between $4t$ and $6.5t$ (well beyond the upper boundary of 4S continuum [$2\pi J (=5.24t)$] [43]) is unique to the doped case. The excitations are bounded by $4t + \pi J\cos(qa/2)$ (dotted red line), which one obtains from a simple convolution of the antiholon and two-spinon excitations. Therefore, we assign these to an antiholon plus two-spinon final state. The fact that the intensity and distribution of these excitations are very sensitive to doping supports this view. As we further increase the doping, we see additional spectral weight above the $4t + \pi J\cos(qa/2)$ boundary, indicating that these quasiparticle interactions are beginning to interact to produce modified dispersion relationships.

3.2.1. Incidence energy dependence

We explore dependence of the RIXS spectra on incident energy considering two values of doping. Figures 4 and 5 show the changes in RIXS intensity maps as the incident photon energy is varied from $\omega_{\text{in}} = -t$ to $4t$ for the 5% and 10% dopings, respectively. The final state excitations resembling $S(q, \omega)$ and $N(q, \omega)$ are clear in all cases, but there are some variations in the overall intensity as ω_{in} is tuned through the XAS resonance peak (figures 4(a) and 5(a), inset). The remaining excitations exhibit a strong incident energy dependence, where both antiholon excitations and the multi-spinon/antiholon excitations centered at $q = 0$ are difficult to resolve for $\omega_{\text{in}} \notin (-t,\ 4t)$.

By varying ω_{in}, one selects particular intermediate states $|n\rangle$ in the RIXS process. The incident energy dependence shown in figures 4 and 5 indicate that only certain intermediate states can reach the multi-particle excitations centered at $q = 0$. The comparison of figure 5 with figure 4 shows that the antiholonic features become more robust wheras the spin excitations are relatively unaffected at each incident energies on increased doping in the 1D chain.

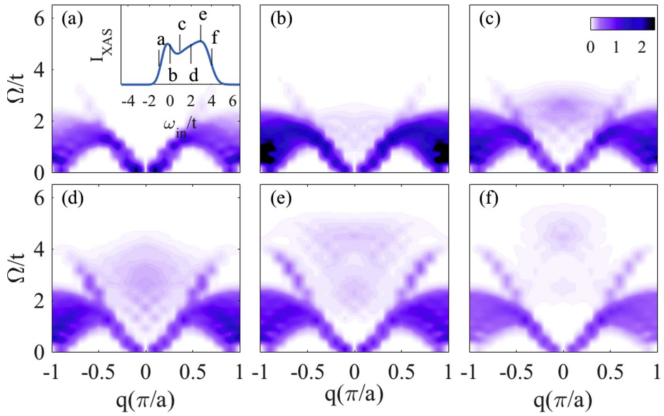

Figure 4. The dependence of RIXS spectra on the incident photon energy ω_{in} for a 5% doped 20-site chain, evaluated using the full Kramers–Heisenberg formalism. The inset of panel (a) shows the XAS spectrum from the model, along with the incident energies used in each of the RIXS calculations.

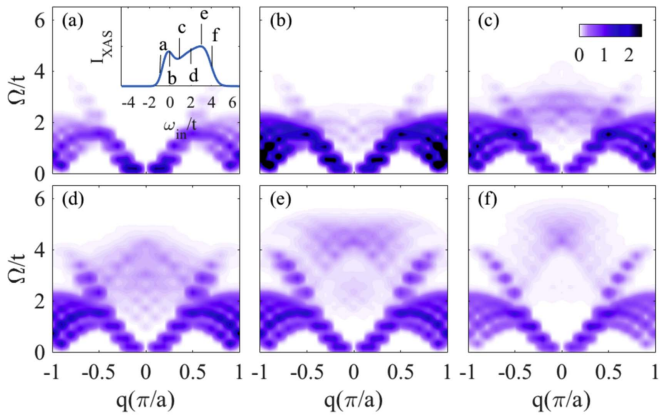

Figure 5. Dependence of RIXS spectra on the incident photon energy ω_{in} for a 10% doped $L = 20$ site chain. The inset of panel (a) shows the XAS spectrum of the same system, along with the incident energies used in each of the RIXS calculations.

3.2.2. Effect of hopping parameter on the RIXS spectra

In this section, we discuss dependence of the RIXS spectra on the hopping parameter t for a fixed J. This analysis helps us further clarify the spin and charge-like nature of the excitations observed in the RIXS spectra. Figure 6 shows two set of excitations: (i) pure magnetic excitations which are insensitive to hopping parameter. In this case, the 2S excitations highlighted by the red solid lines overlay is completely driven by *superexchange* coupling (J). The 4S excitation continuum upper boundary is highlighted by red dotted line. Note that in panels (c) and (d), the 4S continuum is not visible due to our choice of incident energy ω_{in}. In panel (a), the $q = \pi/a$ excitations vanish at $t = 0$. This behavior has also been obtained in [28]. (ii) The dispersion of antiholonic excitations is governed by the hopping amplitude and has a bandwidth of $4t$. The antiholon plus two-spinon continuum ($\bar{h}2S$) is characterized by both the J and t parameters. Indeed, the upper boundary of these excitations is given by $(4t + \pi J\cos(qa/2))$.

4. Discussion and conclusions

Several previous theoretical works have calculated the RIXS spectra for 1D t–J [26, 27] and Hubbard [24, 28] chains using the same formalism. In the doped and undoped cases, these studies obtained RIXS spectra resembling $S(q, \omega)$; however, they did not capture the (anti)holon or multi-spinon excitations observed here. References [26, 28], obtained nonzero weight in the $q = 0$ response but with a significantly reduced spectral weight in comparison to our results. In RIXS at oxygen K-edge, only $\Delta S = 0$ excitations are allowed. References [24, 28] showed that $\Delta S = 0$ excitations vanishes at $q = \pi/a$, whereas we have the maximum at that point in our model. We believe that this discrepancy is due to the lack of hopping from the core-hole site due to the strong core-hole potential used in that work, which is appropriate for the Cu L and K-edges. A strong core-hole

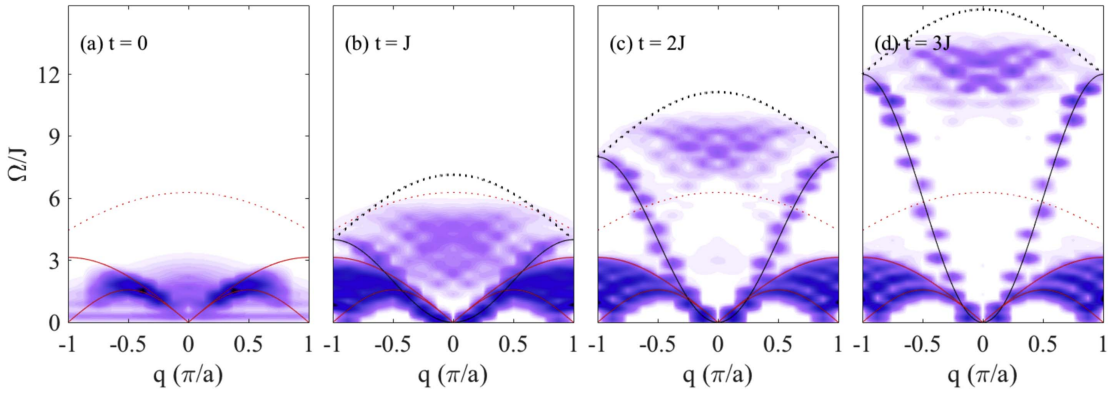

Figure 6. Dependence of the RIXS spectra on the hopping parameter t for a $L = 16$ site doped t–J chain with $\langle n \rangle = 0.94$ doping. The incidence energy, $\omega_{\rm in} = 1.8J,\ \ 3.4J,\ \ 5.6J$ and $7J$ for (a)–(d) panel, respectively. We have chosen these values of the incident energy to highlight the $h2$S continuum portion (absent in $t = 0$ case) of the RIXS spectrum. The spin parts shown with red overlays are insensitive to the hopping, whereas the parts involving antiholon shown with black overlays are directly dependent on the hopping parameter t. Solid and dotted (red) lines report the boundaries of the 2S and 4S continuum, while the solid and dotted (black) show the dispersion of antiholon excitations and upper boundary of antiholon-2S continuum.

potential will tend to localize the excited electrons in the intermediate state, thus suppressing its dynamics. We can confirm this in our model by setting $t = 0$ in the intermediate state for the undoped system, which also prohibits charge fluctuations and produces spectra similar to [24, 28]. Furthermore, given the sensitivity to $\omega_{\rm in}$ shown in figure 4, prior studies may have missed the relevant excitations due to their choice of incident energies.

In RIXS experiment, we expect a uniform modulation of all the excitations in the RIXS intensity given by the angular dependence of the bridging oxygen p_x-orbital [15]. At the oxygen K-edge, 2S, 4S and antiholon are $\Delta S = 0$ excitations without any polarization dependence and hence, one cannot use it to disentangle these excitations. However, 2S and 4S can be disentangled from the antiholonic excitations by making use of the differences in doping dependence of these excitations. One expects that the 2S and 4S will be suppressed upon doping. Instead, the antiholonic features absent in the undoped case, will be enhanced on increased doping.

In summary, we have shown that spin-charge separation can be observed in O K-edge RIXS on doped 1D-AFMs and that these systems exhibit remarkably rich spectra consisting of multi-spinon and holon excitations. Our results highlight the potential for RIXS to simultaneously access the charge, spin, and orbital degrees of freedom in fractionalized quasiparticle excitations, applicable to many quantum materials. Our work provides strong motivation for RIXS experiments at the oxgen K-edge of doped 1D AFMs. The recent RIXS experiment at the O K-edge of undoped Sr_2CuO_3[15] and the availability of doped Sr_2CuO_3 and $SrCuO_2$ crystals [18, 19, 44] demonstrate that our predictions can be verified experimentally in the near future.

Acknowledgments

We thank C D Batista, J Schlappa, T Schmitt, and K Wohlfeld for useful discussions. AN and ED were supported by the US Department of Energy, Office of Basic Energy Sciences, Materials Sciences and Engineering Division. This research used computational resources supported by the University of Tennessee and Oak Ridge National Laboratorys Joint Institute for Computational Sciences.

Appendix A. Effect of $J_{\rm ch}$ at core-hole site on the RIXS spectra

We explore the dependence of RIXS spectra on the value of superexchange interaction $J_{\rm ch}$ in the vicinity of the core-hole. Figure A1 shows that the RIXS spectra, at fixed incident energy, do not depend on $J_{\rm ch}$ qualitatively.

Appendix B. $N(q, \omega)$ of a spinless chain and electron-doped t–J model

We study the dynamical charge structure factor ($N(q, \omega)$) of a t–J chain [45] at small electron *doping* which is similar to the spectrum of a spinless fermion 1D chain with the *same* small fermionic *filling*.

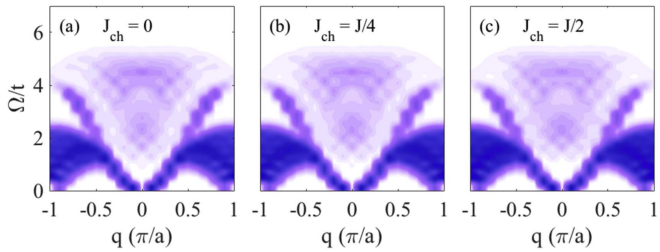

Figure A1. RIXS spectra for different J_{ch} values used in the RIXS intermediate state, with incident energy ω_{in} (=3t).

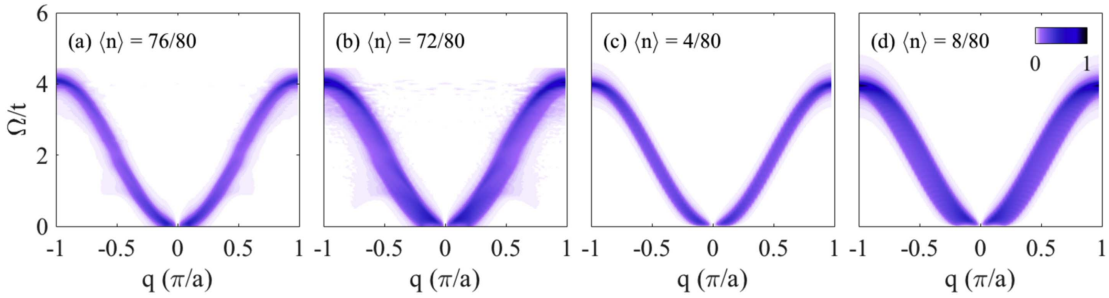

Figure B1. Panels (a) and (b) report the $N(q, \omega)$ for 1D t–J chain with $L = 80$ sites calculated using DMRG at 5% and 10% doping, respectively. Panels (c) and (d) report the $N(q, \omega)$ for *spinless*-fermion 1D chain with $L = 80$ sites computed analytically at 5% and 10% fermionic fillings, respectively.

The $N(q, \omega)$ of a 1D non-interacting spinless fermion chain is given by

$$N(q, \omega) = \sum_{i,j} e^{iq(R_i - R_j)} \langle \psi_g | \hat{n}_j \frac{1}{\omega - \hat{H} + E_{gs} + i\eta} \hat{n}_i | \psi_g \rangle, \tag{B1}$$

where $\hat{n}_i = \hat{c}_i^\dagger \hat{c}_i$ is the fermionic density operator on site i, and η indicates the spectral peaks' broadening. We also denote the ground state as $|\psi_g\rangle = \prod_{|k| \leqslant k_F} \hat{c}_k^\dagger |0\rangle$ with energy E_{gs}, and Fermi momentum $k_F = \pi n$, where $n = N/L$ is the fermionic filling. Focusing on the $q \neq 0$ part, one finds

$$N(q, \omega) = \frac{1}{L} \sum_k \frac{\theta(|k| \leqslant k_F)\theta(|k + q| > k_F)}{\omega - \epsilon_{k+q} + \epsilon_k + i\eta}, \tag{B2}$$

where $\epsilon_k = -2t \cos(k)$ is the dispersion relation for free fermions.

Figure B1 shows explicitly that the $N(q, \omega)$ of the t–J chain at 5% and 10% electron doping computed with DMRG is qualitatively very similar to the results obtained for a spinless fermion chain ($L = 80$ sites) with 5% and 10% fermionic fillings, respectively.

ORCID iDs

Umesh Kumar https://orcid.org/0000-0001-6322-9839

References

[1] Lieb E H and Wu F Y 1968 *Phys. Rev. Lett.* **20** 1445
[2] Kim C, Matsuura A Y, Shen Z-X, Motoyama N, Eisaki H, Uchida S, Tohyama T and Maekawa S 1996 *Phys. Rev. Lett.* **77** 4054
[3] Segovia P, Purdie D, Hengsberger M and Baer Y 1999 *Nature* **402** 504
[4] Fujisawa H, Yokoya T, Takahashi T, Miyasaka S, Kibune M and Takagi H 1999 *Phys. Rev.* B **59** 7358
[5] Kim B J *et al* 2006 *Nat. Phys.* **2** 397
[6] Koitzsch A, Borisenko S V, Geck J, Zabolotnyy V B, Knupfer M, Fink J, Ribeiro P, Büchner B and Follath R 2006 *Phys. Rev.* B **73** 201101
[7] Jompol Y, Ford C J B, Griffiths J P, Farrer I, Jones G A C, Anderson D, Ritchie D A, Silk T W and Schofield A J 2009 *Science* **325** 597
[8] Ament L J P, van Veenendaal M, Devereaux T P, Hill J P and van den Brink J 2011 *Rev. Mod. Phys.* **83** 705
[9] Hill J P *et al* 2008 *Phys. Rev. Lett.* **100** 097001
[10] Dean M P M *et al* 2013 *Phys. Rev. Lett.* **110** 147001
[11] Ament L J P, Ghiringhelli G, Sala M M, Braicovich L and van den Brink J 2009 *Phys. Rev. Lett.* **103** 117003
[12] Schlappa J *et al* 2012 *Nature* **485** 195138
[13] Wohlfeld K, Nishimoto S, Haverkort M W and van den Brink J 2013 *Phys. Rev.* B **88** 195138

[14] Kojima K M et al 1997 Phys. Rev. Lett. 78 1787
[15] Schlappa J et al 2018 arXiv:1802.09329
[16] White S R 1992 Phys. Rev. Lett. 69 2863
[17] White S R 1993 Phys. Rev. B 48 10345
[18] Karmakar K, Bag R and Singh S 2015 Cryst. Growth Des. 15 4843
[19] Karmakar K, Bag R, Skoulatos M, Rüegg C and Singh S 2017 Phys. Rev. B 95 235154
[20] Ament L J P 2010 PhD Thesis Univeriteit Leiden, Netherlands https://openaccess.leidenuniv.nl/handle/1887/16138
[21] Neudert R et al 2000 Phys. Rev. B 62 10752
[22] Walters A C, Perring T G, Caux J-S, Savici A T, Gu G D, Lee C-C, Ku W and Zaliznyak I A 2009 Nat. Phys. 5 867
[23] Lee W S et al 2013 Phys. Rev. Lett. 110 265502
[24] Igarashi J-I and Nagao T 2012 Phys. Rev. B 85 064422
[25] Tohyama T and Tsutsui K 2018 Int. J. Mod. Phys. B 32 1840017
[26] Ament L J P, Forte F and van den Brink J 2007 Phys. Rev. B 75 115118
[27] Klauser A, Mossel J, Caux J-S and van den Brink J 2011 Phys. Rev. Lett. 106 157205
[28] Kourtis S, van den Brink J and Daghofer M 2012 Phys. Rev. B 85 064423
[29] Forte F, Cuoco M, Noce C and van den Brink J 2011 Phys. Rev. B 83 245133
[30] Eskes H and Jefferson J H 1993 Phys. Rev. B 48 9788
[31] Popović Z V et al 2001 Phys. Rev. B 63 165105
[32] Kühner T D and White S R 1999 Phys. Rev. B 60 335
[33] Jeckelmann E 2002 Phys. Rev. B 66 045114
[34] Nocera A and Alvarez G 2016 Phys. Rev. E 94 053308
[35] Alvarez G 2009 Comput. Phys. Commun. 180 1572
[36] Mourigal M, Enderle M, Klopperpieper A, Caux J-S, Stunault A and Ronnow H M 2013 Nat. Phys. 9 435
[37] Kim Y-J et al 2004 Phys. Rev. Lett. 92 137402
[38] Woynarovich F 1982 J. Phys. C: Solid State Phys. 15 85
[39] Ogata M and Shiba H 1990 Phys. Rev. B 41 2326
[40] Penc K, Hallberg K, Mila F and Shiba H 1997 Phys. Rev. B 55 15475
[41] Sorella S and Parola A 1992 J. Phys.: Condens. Matter 4 3589
[42] Kim C, Shen Z-X, Motoyama N, Eisaki H, Uchida S, Tohyama T and Maekawa S 1997 Phys. Rev. B 56 15589
[43] Caux J-S and Hagemans R 2006 J. Stat. Mech. P12013
[44] Simutis G et al 2013 Phys. Rev. Lett. 111 067204
[45] Deisz J, Luk K-H, Jarrell M and Cox D L 1992 Phys. Rev. B 46 3410